Integrated 64-Channel Spatiotemporally Patterned Multipolar Neural Stimulator with 150nA–10mA Current Range at 8V–20V Voltage Compliance

Jeong-Hoon Kim*, Min Suk Lee*, Yongjae Park†, Jiajia Wu*, Zhaoyi Liu*, Cassia Rizq*, Preston Fowler*, Abhinav Uppal*, Omowuyi Olajide*, Athena Leisching*, Abraham Akinin§, Lara M. Rangel*, Seong-Jin Kim‡, and Gert Cauwenberghs*

*University of California San Diego, CA, USA, †Ulsan National Institute of Science and Technology, Ulsan, Korea, ‡Sogang University, Seoul, Korea, §Lawrence Livermore National Laboratory, CA, USA

j4kim@ucsd.edu and gcauwenberghs@ucsd.edu

***Abstract*—This work presents a 64-channel current-mode neural stimulator with 96 dB current dynamic range from 150 nA to 10 mA and voltage compliance ranging from 8 V to 20 V. Each channel supports dynamically configurable arbitrary spatiotemporal stimulation profiles through a 10-b DAC temporal envelope at 125 ksps and a 6-b spatial per-channel multiplying gain over a programmable SPI. Fabricated in 180 nm HV BCD technology, the stimulator demonstrates $<2\%$ variation across the current range under dynamic supply voltage scaling from ± 5.5 V to ± 12 V and <5 mV residual voltage through active shunt charge balancing for monopolar, bipolar, and multipolar stimulation modes. Benchtop and ex-vivo tests demonstrate multipolar stimulation and flexible interfacing with both micro- and macroelectrodes, validating compatibility with microscale experimental setups and high-current clinical stimulation protocols.**

***Index Terms*—Implantable Bioinstrumentation, Neuromodulation, CCS, Multipolar Stimulation, Charge Balancing**

I. Introduction

Neural stimulation spans preclinical research and therapeutic applications, with deep brain stimulation (DBS) and spinal cord stimulation (SCS), successfully treating disorders such as Parkinson's disease and chronic pain [1], [2]. Among various neural stimulation methods, current-controlled stimulation (CCS) is widely used because of its precise regulation and estimation of delivered charge via control of current amplitude and pulse duration. Depending on the experimental purpose, stimulation electrode types can range from microelectrodes to macroelectrodes, and the required stimulation current may vary from hundreds of nanoamperes (nA) in preclinical animal model studies [3] to tens of milliamperes (mA) in high-current applications such as DBS and SCS [1], [2]. In particular, high-impedance microelectrodes can result in large voltage drops across the electrode–tissue interface, even at very low current levels, potentially exceeding the compliance voltage of the stimulator. Furthermore, accurate charge balancing is critical to prevent residual charge buildup [4].

Here, we present a 64-channel neural stimulator implemented in a 180 nm high-voltage Bipolar-CMOS-DMOS (HV BCD) process, supporting a wide current range from sub-μA to 10 mA and a compliance voltage of up to 20.56 V. Each stimulator channel is independently programmable and supports spatiotemporal control of current intensity, enabling the application of arbitrary stimulation waveforms for monopolar to multipolar electrode configurations. The addition of an active shunt switch with adjustable driving strength ensures accurate charge balancing and calibration capabilities. Overall, the proposed system shows great compatibility and configurability for a broad range of neuromodulation applications with various types of electrodes.

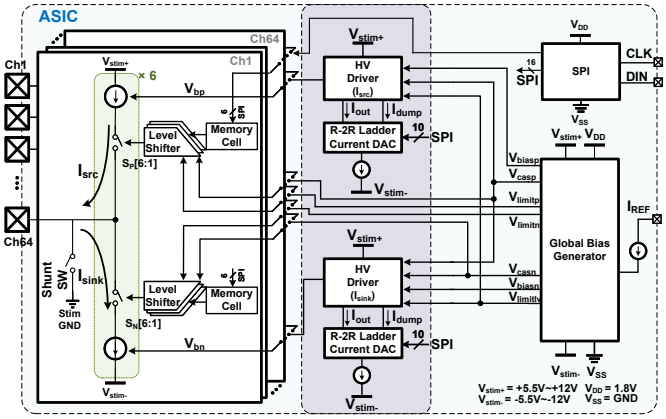

Fig. 1. Architecture of the 64-channel stimulator ASIC with R-2R MOS DACs, HV drivers, and per-channel memory for precise, wide dynamic range programmable current stimulation.

II. Hardware Implementation

A. System Overview

The overall architecture is shown in Fig. 1. A global analog bias generator is shared by two source/sink digital-to-analog converters (DACs) and HV drivers to ensure consistent characteristics of the analog front-end circuits. The on-chip serial-parallel interface (SPI) receives external configuration data for spatiotemporal control over individual 64 channels of the current stimulator. Temporal control of current stimulation is achieved by adjusting a time-varying current envelope through the 10-b DACs, whereas each of the 64 channels includes an 8-

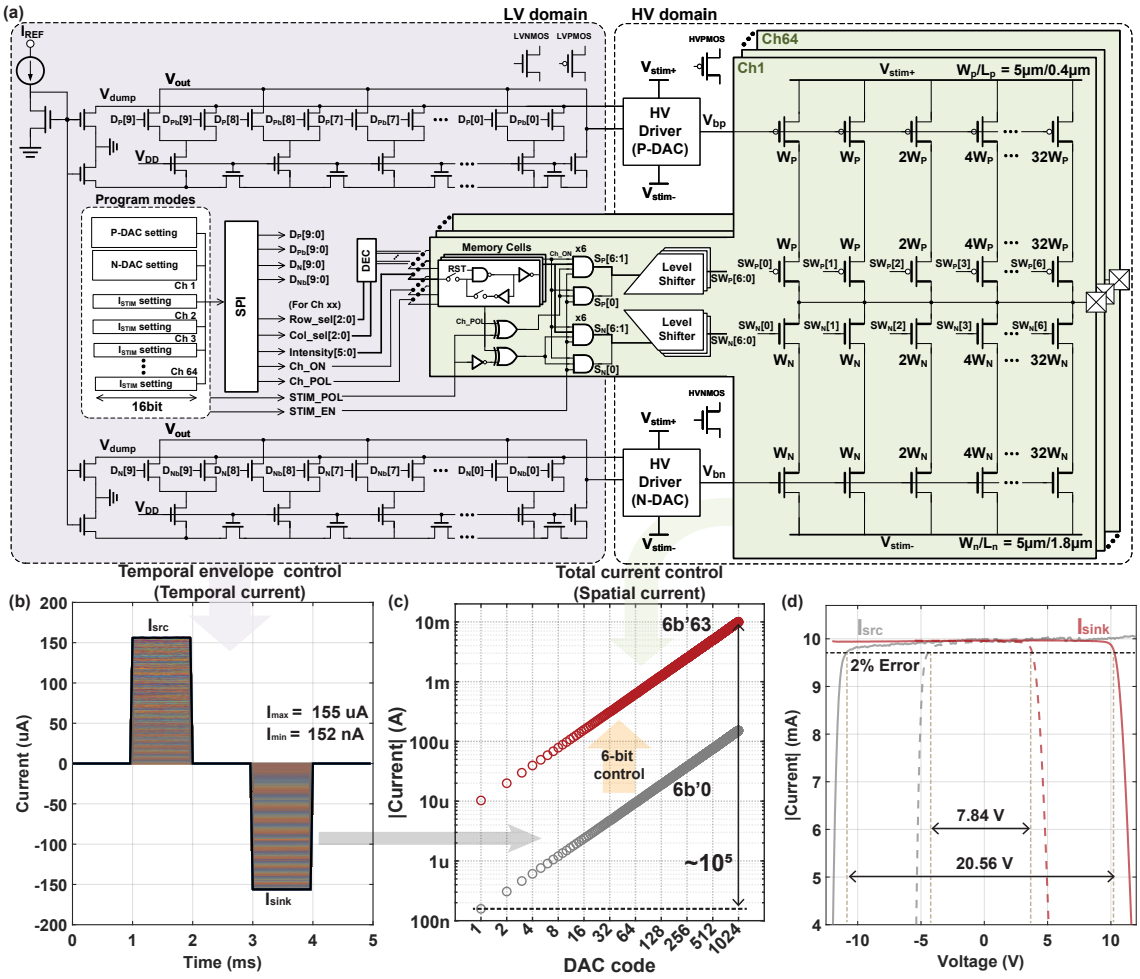

Fig. 2. (a) Circuit schematic of 64-channel spatiotemporally programmable wide-range current stimulator, implemented with 10-b R-2R MOS DACs for current envelope control and channel-specific 6-b controlled current scaling branches. (b) Measured temporal current envelope across the 10-b DAC range at unity spatial scaling. (c) Measured spatial scaling of peak envelope currents across the 6-b scaling range. (d) Measured compliance voltage across $\pm$12V and $\pm$5.5V supply voltages.

b memory cell for channel-specific spatial patterning, with 6-b amplitude control modulating total current by selecting current scaling branches. The remaining 2 bits are for activating the channel and controlling its polarity, allowing for cathodic/anodic patterning in addition to multiphasic sequencing. After stimulation, a shunt switch may be activated as needed to achieve precise charge balancing.

B. Spatiotemporally Programmable Current Stimulator

Fig. 2(a) illustrates the circuit schematic of the current stimulator capable of spatiotemporal control of current stimulation over a wide dynamic range from 150 nA to 10 mA. To precisely adjust the current envelope stimulation level, we adopt a global 10-b R-2R MOS ladder DAC using low-voltage (LV) devices at 125 ksps. The reference current I_{REF} is first delivered to the DAC through a current mirror and is selectively scaled according to the 10-b digital code received via SPI. The current selectively scaled by the DAC is then converted to bias voltagesV_{bp} and V_{bn} through the HV drivers and globally distributed to all 64 channels. To maintain linearity and accuracy, the current from unselected DAC branches is routed to a dumping path to prevent interference with the output current.

As shown in Fig. 2(b), this architecture enables precise temporal control of current envelope, achieving current envelope levels ranging from 152 nA to 155 µA. As shown in Fig. 2(c), once the current envelope is defined by the sink/source DAC, each current stimulator independently adjusts its total stimulation current by selecting binary-weighted current stimulator branches based on 6-b data stored in local memory cells. Each branch contributes to form the total stimulation current by scaling the current envelope defined by the DAC. With this spatiotemporal current control, the system supports a wide current dynamic range from sub-µA to 10 mA ($\sim$96 dB). Independent current control per stimulator enables us to achieve spatially patterned stimulation and various stimulation configurations from monopolar to multipolar. Notably, multipolar stimulation effectively suppresses stimulation-induced

artifacts [5] and common-mode voltage excursion [6], thereby improving neural recording performance in the closed-loop system.

Due to the current mirror-based global bias generation circuit and DAC architecture, the supply voltage can be dynamically scaled from $\pm 5.5\,\mathrm{V}$ to $\pm 12\,\mathrm{V}$ variable voltage supplies while maintaining a maximum stimulation current of $10\,\mathrm{mA}$. This dynamic voltage supply configuration reduces the energy overhead and enables energy-efficient operation by adapting the supply voltage to the application's compliance requirements [7]. In Fig. 2(d), the compliance voltage was measured at the electrode node where the stimulation current dropped by 2%. The measured compliance voltage can be scaled from $7.84\,\mathrm{V}$ at $\pm 5.5\,\mathrm{V}$ to $20.56\,\mathrm{V}$ at $\pm 12\,\mathrm{V}$. At the maximum output current of $10\,\mathrm{mA}$, the current error is less than 2% over the compliance voltage ranges, demonstrating highly stable stimulation performance and the potential for power savings across different stimulation applications.

C. Active Shunt Switch

As shown in Fig. 3(a), in the conventional CCS method, biphasic current stimulation is adopted to ensure zero net charge injection using a pair of cathodic and anodic phases. However, current mismatches in the stimulator and non-ideal capacitive behavior of the electrode can induce the residual voltage on the electrode after stimulation. This residual voltage may accumulate over consecutive stimulation cycles, resulting in a DC offset that may cause tissue damage or electrode degradation when it exceeds the safety limit [4].

Since most of the injected charge is canceled by the biphasic stimulation itself, passive shunt switches have been widely adopted as the simplest circuit-level solution to discharge residual voltage on the electrode [8], [9]. However, with a passive shunt method, the charge balancing duration is determined by the electrode capacitance and the switch on-resistance, which can limit the stimulation frequency. This becomes problematic in high-frequency applications, where insufficient discharge time may result in incomplete charge removal and limited stimulation rate. Furthermore, passive switches have a limited operating voltage range, making them unsuitable for handling large voltage swings at the electrode node.

To overcome these limitations, we implemented an active shunt switch using HV devices, enabling high-speed charge balancing independent of electrode properties. The proposed circuit drives four times the reference current I_{shunt} through a current mirror to actively remove the residual voltage on the electrode. Fig. 3(b) shows that charge balancing duration can be modulated through driving strength adjustment, independent of the electrode capacitance. $1\,\mu\mathrm{F}$ and $200\,\mathrm{nF}$ capacitors precharged to $2\,\mathrm{V}$ were discharged within a comparable duration using $50\,\mu\mathrm{A}$ and $10\,\mu\mathrm{A}$ driving currents, respectively. Moreover, in applications requiring high stimulation frequencies, the discharge speed can be further enhanced by increasing the driving strength. As shown in Fig. 3(c), the active shunt switch can drive any voltage within the compliance range to

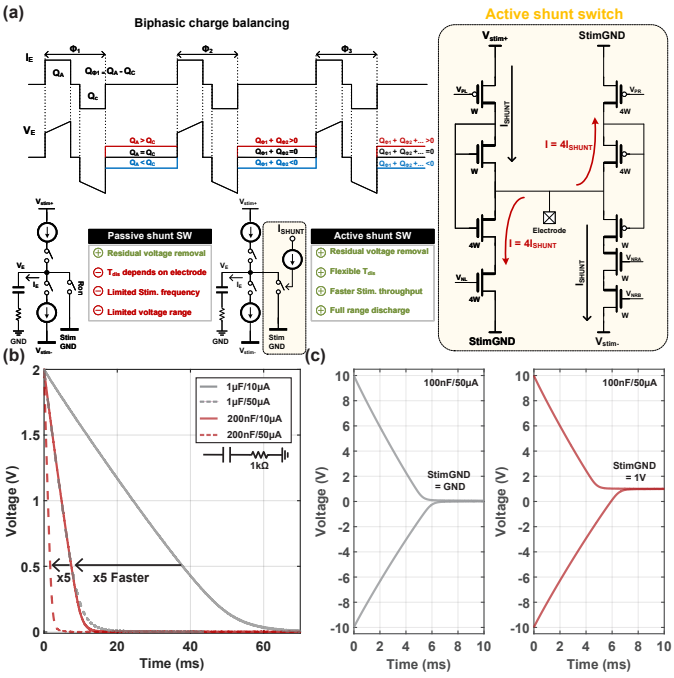

Fig. 3. (a) Conventional limitation in CCS using biphasic stimulation and circuit schematic of proposed charge balancing method, active shunt switch. (b) Measured Active shunt switch with tunable discharge strength with various electrode loads. For the electrode load: 1 µF or 200 nF with I_{shunt} of 10 µA or 50 µA. (c) Measured full-range residual voltage removal with externally defined StimGND.

the StimGND level. The ability to set StimGND with external reference voltages enables not only accurate charge balancing but also interfacing with heterogeneous systems, such as neural recording systems.

III. Experimental Results

Fig. 4 shows the chip micrograph of the proposed chip implemented in a $180\,\mathrm{nm}$ HV BCD process with the total area of $16\,\mathrm{mm}^2$ for 64 current stimulator and $0.154\,\mathrm{mm}^2$ for the single current stimulator including the pads. A detailed comparison of related works and performance metrics are summarized in Table I.

Fig. 5(a) and (b) show experiments that emulate the monopolar stimulation using a single electrode modeled as a $100\,\mathrm{nF}$ capacitor in series with a $1\,\mathrm{k}\Omega$ resistor under $1\,\mathrm{mA}$ biphasic current stimulation. During 300 consecutive stimulations, residual voltage $2.8\,\mathrm{mV}$ per stimulation cycle was observed, which indicates a high precision of the current matching (0.26% mismatch) during the anodic and cathodic phases. However, even under very small mismatch, the residual voltage can easily exceed the safety limit after consecutive stimulations. Under the same conditions, enabling the proposed active shunt switch reduced the residual voltage to below $5\,\mathrm{mV}$, confirming the system's capability to achieve precise charge balancing. To validate the practical applicability of the system, both bench-top and ex-vivo experiments were conducted using macroelectrodes and microelectrodes, respectively. In the bench-top testing shown in Fig. 5(c),

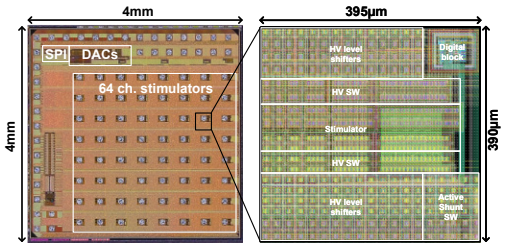

Fig. 4. Chip micrograph

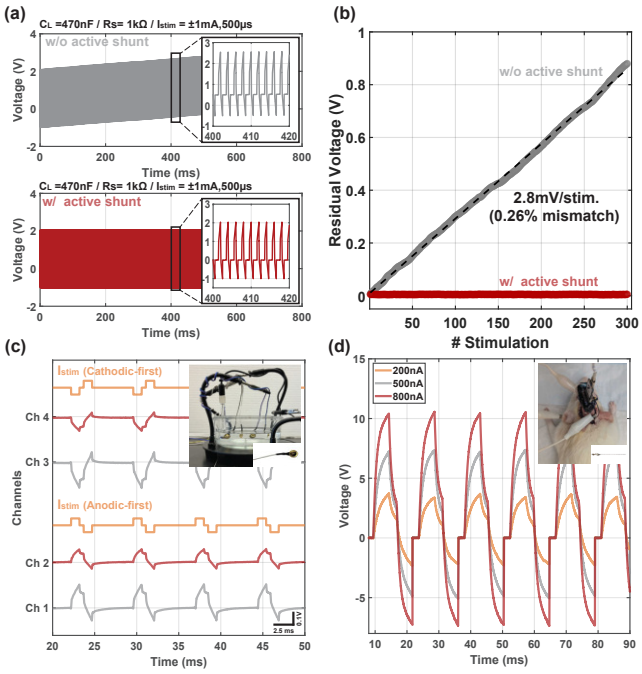

Fig. 5. (a) Measured electrode voltage without active shunt (top) and with the shunt (bottom) under 300 cycles of 1 mA biphasic monopolar stimulation with 500 µs cathodic and anodic phases; the electrode model consists of a 470 nF capacitor and 1 kΩ resistor in series. The applied I_{shunt} = 10 µA. (b) Extracted residual voltage 500 µs after each biphasic pulse, comparing cases with and without the active shunt. (c) Measured stimulation voltage in Phosphate Buffered Saline (PBS). Ch 1,2 and Ch 3,4 display stimulation recordings of anodic-first and cathodic-first current stimulation, respectively. Current waveform is represented in color orange. Red and grey signals are measured under biphasic stimulation currents of 0.44 mA and 0.85 mA, respectively. (d) Monopolar biphasic stimulation of rat brain tissue for three different current amplitudes (200 nA, 500 nA, and 800 nA) through a tungsten stimulation electrode (inset) with a skull screw over cerebellum as stimulation ground.

four Au-based macroelectrodes were used to demonstrate multipolar stimulation where current levels and polarity can be independently controlled. In ex-vivo testing shown in Fig. 5(d), continuous low-current (200 – 800 nA) stimulation pulses were applied using high-impedance microelectrodes. The residual voltage remained within safe operating limits, confirming reliable operation in biological environments.

IV. Conclusion

We presented a 64-channel neural stimulator fabricated in a 180 nm HV BCD process, supporting a wide current dynamic range from 150 nA to 10 mA and a high compliance voltage up to 20 V. The system enables flexible, spatiotemporal control of stimulation through a 10-b current envelope scaling combined with per-channel 6-b current scaling. Dynamic voltage supply scaling from ±5.5 V to ±12 V is supported to enable energy-efficient load-dependent operation. The proposed active shunt switch ensures precise charge balancing across various stimulation scenarios with high-frequency and high-impedance. This work provides a scalable and programmable stimulation platform suitable for a wide range of neurostimulation applications.

TABLE I
Comparison of Current Stimulator Circuits.

Publication	JSSC'22 [5]	CICC'24 [10]	CICC'21 [6]	TBCAS'21 [9]	JSSC'23 [8]	This Work
Technology	180nm HV	180nm LV	180nm HV	180nm LV	250nm	180nm HV BCD
Stimulation Type	CCS	CCS	CCS	CCS	CCS	CCS
Supply Voltage	1.8V/5V	3.3V – 11V	14V	±6V	1.8V/2.5V/ 3.75V/5V	±5.5V– ±12V
Compliance Voltage	40V	4.9V– 20V	26V	<12V	5V	7.84V/20.56V
Stimulation Range	<12.75mA	<3.5mA	<2mA	200µA – 3.2mA	150nA – 2.5µA (9.6µA– 160µA)[b]	152nA – 10mA
Resolution	8 bit	N.A.	7 bit	4 bit	6 bit	10 bit (Temporal) + 6 bit (Spatial)
# of channels / # of stimulators	16/4	8/N.A.	46/46	8/1	505/101	64/64
Area/channel	1.71 mm²	0.06 mm²	0.12 mm²	0.08 mm²	0.01 mm²	0.154 mm²
Charge Balancer	TBCB	N/A	CIC+RIC	Passive	Passive	Active Shunt
Residual Voltage	<2mV	<35mV	<50mV	2.1mV [a]	N.A.	<5mV
V_{CM} excursion	N.A.	No	Yes	No	No	Yes
Stimulation Waveform	Rectangle	Arbitrary	Arbitrary	Rectangle	Rectangle	Arbitrary
Stimulator Configuration	Monopolar – Multipolar	Bipolar (H-bridge)	Vector Stimulation	Monopolar	Bipolar	Monopolar – Multipolar

a: Before passive CB b: Adjustable range with serial communication

V. Acknowledgment

LLNL was supported by DE-AC52-07NA27344 and NIH contract ADC15001001-1-0-1.

References

[1] A. L. Benabid, S. Chabardes *et al.*, "Deep brain stimulation of the subthalamic nucleus for the treatment of parkinson's disease," *The Lancet Neurology*, vol. 8, no. 1, pp. 67–81, 2009.

[2] A. Rowald, S. Komi *et al.*, "Activity-dependent spinal cord neuromodulation rapidly restores trunk and leg motor functions after complete paralysis," *Nature Medicine*, vol. 28, no. 2, pp. 260–271, 2022.

[3] S. Ronchi, M. Fiscella *et al.*, "Single-cell electrical stimulation using CMOS-based high-density microelectrode arrays," *Frontiers in Neuroscience*, vol. 13, p. 208, 2019.

[4] S. F. Cogan, "Neural stimulation and recording electrodes," *Annual Review of Biomedical Engineering*, vol. 10, no. 1, pp. 275–309, 2008.

[5] H. Pu, O. Malekzadeh-Arasteh *et al.*, "A CMOS dual-mode brain-computer interface chipset with 2-mV precision time-based charge balancing and stimulation-side artifact suppression," *IEEE J. Solid-State Circuits*, vol. 57, no. 6, pp. 1824–1840, 2022.

[6] A. Mandal, D. Peña *et al.*, "A 46-channel vector stimulator with 50mV worst-case common-mode artifact for low-latency adaptive closed-loop neuromodulation," in *2021 IEEE Custom Integrated Circuits Conference (CICC)*, 2021, pp. 1–2.

[7] Y. You, R. Tian *et al.*, "A high-voltage-compliant 86% peak efficiency current-mode stimulator with dynamic voltage supply for implantable medical devices," *IEEE Journal of Solid-State Circuits*, pp. 1–13, 2024.

[8] K. Eom, M. Park *et al.*, "A low-stimulus-scattering pixel-sharing sub-retinal prosthesis SoC with time-based photodiode sensing and per-pixel dynamic voltage scaling," *IEEE J. Solid-State Circuits*, vol. 58, no. 11, pp. 2976–2989, 2023.

[9] C.-C. Hsieh and M.-D. Ker, "Monopolar biphasic stimulator with discharge function and negative level shifter for neuromodulation SoC integration in low-voltage CMOS process," *IEEE Trans. Biomed. Circuits Syst.*, vol. 15, no. 3, pp. 568–579, 2021.

[10] J. Wie, S. Jung *et al.*, "A 3.3-to-11V-supply-range 10μW/Ch arbitrary-waveform-capable neural stimulator with output-adaptive-self-bias and supply-tracking schemes in 0.18μm standard cmos," in *2024 IEEE Custom Integrated Circuits Conference (CICC)*, 2024, pp. 1–2.